Photomultipliers and Microchannel Plates

IEEE Transactions on Nuclear Science, Vol. NS-29, No. 1, February 1982

EVALUATION OF THE NEW GENERATION RCA 8854 PHOTOMULTIPLIER

C.C. Lo, Branko Leskovar
Lawrence Berkeley Laboratory
University of California
Berkeley, California 94720 U.S.A.

Abstract

Characteristics have been measured for the new generation RCA 8854 114 mm-diameter photomultiplier. The first dynode of this photomultiplier has a cesium-activated, gallium-phosphide secondary emitting surface. Some typical photomultiplier characteristics--such as gain, dark current and risetime--are compared with data provided by the manufacturer. Photomultiplier characteristics generally not available from manufacturer were also measured. These include pulse height spectrum and time spectrum of afterpulses. In addition, measurements have been made of the collection and quantum efficiency uniformity and of the single photoelectron time spread for the full photocathode illumination. Measurement techniques and description of measuring systems are given in detail.

Introduction

The RCA 8854 is a variant of the 4522. It has a high gain GaP first dynode followed by thirteen BeO dynodes. The new RCA designation for the photocathode is 35ET (formerly 118), which has a peak response at 400 nm and a quantum efficiency of 27%. Its spectral response extends from 200 nm to 660 nm. The minimum useful photocathode diameter is 114 mm. The anode output pulse (10-90%) risetime is approximately 3 ns.

Several specific measurements were made related to a possible application of the photomultiplier in the Deep Underwater Muon and Neutrino Detection (DUMAND) system. The DUMAND Project proposes to study muon and neutrino interactions at ultra-high energies and to investigate astronomical phenomena by means of neutrinos which reach the earth from extra-terrestial sources.

The proposed technique involves creating a large target-detector system, consisting of 1 km^3 of seawater at a deep ocean site. The thick layer of ocean above the target-detector system will significantly reduce the intense background of cosmic ray muons produced in the earth's atmosphere. A three-dimensional array of photon detectors, consisting of approximately 22×10^3 or 44×10^3 photomultipliers will detect Cerenkov light resulting from particle cascades in the deep detection volume. Photomultipliers will be housed in optical sensor modules together with appropriate fluorescent wavelength shifters. The modules will be deployed on vertical strings, which will be connected to one another at the ocean floor. Earlier DUMAND workshops (1,2,3) described the optical array system and its characteristics with respect to the array efficiency for observation of both hadronic cascades and muon tracks which result from arriving neutrinos. Also, the photomultiplier characteristics for the DUMAND system were analyzed in general terms in an earlier paper (4). These efforts and the considerations presented at the DUMAND Signal Workshop, February 11-16, 1980, pointed out the need to make pulse height resolution and afterpulse measurements of the RCA 8854.

Standard tests, such as gain and dark current as a function of supply voltage, were carried out to make sure that the photomultipliers were performing normally before any other tests were made. Specific tests, such as photocathode uniformity, dark pulse spectrum, pulse height resolution and afterpulse frequency, were performed at room temperature.

Figure 1 shows the schematic diagram of the divider used for all the measurements. When operating the focus electrode at the same potential as the first dynode, all three 8854's showed the best collection efficiency.

Gain and Dark Current Measurements

Gain and dark current measurements were made with the system described in Ref. 5. Figure 2 shows the average gain and dark current characteristics of the three photomultipliers tested, as a function of voltage applied between the anode and cathode. With 2500 V applied between the anode and cathode, the gain was 3.5×10^8, while the dark current was 1.30×10^{-7}A.

Collection and Quantum Efficiency Uniformity Measurements

A system similar to the one described in Ref. 6 was used to measure collection and quantum efficiency uniformity. The results of two of the three 8854 photomultipliers are presented in this report. Figures 3 and 4 show that the uniformity is better than 50% within a 5 cm radius from the center of the photocathode. This is a marked improvement over the development type C70133B photomultipliers (9).

Pulse Height Resolution Measurement

The system used to measure resolution was similar to the one described in Ref. 7. The first peak-to-valley ratio of the three photomultipliers ranges from 1.6 to 1.9. Figure 5 shows the pulse height spectrum of 8854, serial number 1337, with the first peak-to-valley ratio of 1.9 : 1. The dark pulse spectrum of the same 8854 is shown in Figure 6. The average dark pulse count of the three 8854's, summing from 1/8 photoelectron to 16 photoelectron, is

$$\sum_{1/8\ \text{photoelectron}}^{16\ \text{photoelectron}} = 155 \text{ counts per second}$$

Afterpulse Measurements

Contemporary fabrication and activation techniques have reduced afterpulses from most photomultipliers to a point where they are rarely important. However,

0018-9499/82/0200-0184$00.75

for the large photocathode area photomultipliers for the DUMAND detection system, a significant amount of afterpulses could introduce serious error. One group of afterpulses may be produced as a result of the ionization of residual gases, such as He, H_2, N_2 and CO, between the photocathode and the first dynode (8). The positive ions formed are accelerated toward the photocathode by the focusing electric field. On impact these ions liberate up to five secondary electrons which constitute the secondary signal or afterpulse. These afterpulses generally occur from 200 ns to several microseconds after the main pulse. The time of occurence of the afterpulses can be closely correlated with the atomic mass of the residual gas inside the glass envelope. Other phenomena may cause afterpulsing, such as dynode fluorescence, electrical fields in the exposed glass of the envelope, etc. In order to measure this characteristic, a pulse height spectrum and a time spectrum must be taken of the anode output pulse. Figure 7 is a block diagram of the system for measuring the pulse height spectrum.

A pulse generator was used to drive a light-emitting diode, type XP 21. The light intensity of the pulse was controlled by varying the drive pulse amplitude. The light-emitting diode was placed more than 1 meter away from the photocathode of the photomultiplier. An attenuator and preamplifier were used at the output of the photomultiplier to provide more flexibility for controling pulse height spectrum display on the pulse height analyzer.

Table 1 shows the dark pulse count of three 8854's from 1/8 photoelectron to 16 photoelectron and also at various photoelectron peaks to 16 photoelectron level, inclusive. An obvious conclusion is that most of the dark pulses are of single electron. Only a few percent of dark pulses are of two photoelectron and above. These are probably quite different in origin from the single electron pulses. The dark pulse count of the three 8854's ranges from 137 counts per second to 207 per second by summing all pulses between 1/8 photoelectron to 16 photoelectron. Figure 6 shows a typical dark pulse height spectrum of an 8854.

Table 2 shows the results of the high counting rate measurement. On this measurement a light-emitting diode was pulsed at 1 MHz and the light level was adjusted so that the 8854 yielded 100 kHz of single photoelectron pulses. Note that the 100 kHz pulse frequency was limited by the pulse height analyzer used in the measuring system. Under high, single photoelectron counting operation the percentage of pulses of two photoelectron and above is very similar to that in the dark counting measurement. However, it is interesting to note that the percentage of pulse count of three photoelectron and above was smaller than in the dark pulse count case. It appears that this effect is caused by a gain decrease of the photomultiplier operating at the signal induced condition and by statistical error of the measurement. Figure 9 shows a typical pulse height spectrum of an 8854 under 100 kHz single photoelectron counting operation.

The system shown in Figure 8 was used to measure afterpulses. A pulse generator was used to drive a light-emitting diode, type XP 21, which, in turn, produced light pulses for the photomultiplier. The trigger pulse from the pulse generator was delayed and shaped before it was used as a start pulse for the time-to-amplitude converter (TAC). The output pulse of the photomultiplier was used as the stop pulse for the TAC after being processed by the constant fraction discriminator. The trigger pulse from the pulse generator, however, was purposely delayed to come after the photomultiplier main pulse so that an output pulse from the TAC would only occur when the photomultiplier generated an afterpulse. The output of the TAC was then recorded and displayed on the pulse height analyzer. In order to look for pulses many microseconds after the main pulse, the timing range of the TAC must be set accordingly and unavoidably limit the operating frequency of the test system. Table 3 shows the results of the afterpulse measurement.

Under single photoelectron counting at a rate of 100 kHz afterpulses were detected in the time interval ranges of 52 - 58.5 ns and 190 - 192 ns, after the main output pulse in all three photomultipliers. In the 450 ns - 68 μs time range afterpulses were detected in two out of three 8854's. For one photomultiplier at a 10 kHz pulse rate, 0.8 afterpulses per second were observed at 933 ns and the other at 1 kHz pulse rate gave 3.4 afterpulses per second at 12.5 μs.

When the light pulse intensity was increased so that pulses with three photoelectrons were produced by the 8854's afterpulses were detected in four time intervals in all three photomultipliers: 54.5 - 59 ns, 197 - 198 ns, 956 - 987 ns, and 10.6 - 12.8 μs. Detailed results are given in table 3.

Figure 10 shows the time distribution of output pulses in the time interval 0 - 150 ns after the main photomultiplier pulse under a 100 kHz single photoelectron counting rate. The first distribution at the begining of the spectrum is the main output pulse of the photomultiplier. The second distribution represents the afterpulses which occured 52 - 58.6 ns time interval after the main pulse.

Figure 11 shows the afterpulse spectrum in the time interval 4.5 - 68 μs under 10 kHz-three photoelectron counting rate (limited by TAC timing range setting). Afterpulses were present in all three photomultipliers at 8.5 μs, 9.2 μs, 12.8 μs and 14 μs after the main photomultiplier output pulse.

The pulse height spectrum shown in Fig. 9 indicates that very few pulses were above the 4 photoelectron level and most of the pulses were well below level.

Single Photoelectron Measurements

There are generally two important parameters regarding single photoelectron operation of photomultipliers; namely, (1) the pulse response and (2) the time resolution. Both parameters were measured with the systems described in Ref. 4.

Figure 12 shows the output pulse of an 8854 operating at the single photoelectron level. The 10 - 90% risetime of the pulse is 3.2 ns, and its full-width at half-maximum is 4 ns.

Figure 13 shows two single photoelectron time spread spectra spaced 16 ns apart. The full-width at half-maximum time spread was 1.55 ns with the full photocathode illuminated. When a 3.2 mm diameter spot was illuminated at the center of the photocathode, the time spread became 1.35 ns.

Conclusions

Measurements have shown that the basic characteristics of the 8854 photomultipliers agree closely with those given by the manufacturer. The photocathode uniformity as well as the pulse height resolution were found to be significantly better than the developmental

type C70133B, (9).

Dark pulse spectra of the three 8854's measured showed that the average pulse count from 2 - 16 photoelectron, inclusive, was 4.6% and that from 3 - 16 photoelectron, inclusive, was 3.6%. Under 100 kHz signal-induced counting rate, the average pulse count from 2 - 16 photoelectron, inclusive, was 4.9% and that from 3 - 16 photoelectron, inclusive, was 0.58%. 96.4% of the pulses in the dark spectrum were below 3 photoelectron, whereas 99.4% of the pulses in the 100 KHz signal-induced spectrum were below 3 photoelectron. Thus, it appears that the dark pulse spectrum includes both multielectron and single electron pulses.

Afterpulses were detected under single photoelectron counting at 52 - 59 ns and 190 ns in all three tubes, 933 ns in one and 12.5 μs in another. By increasing the pulse height to a predominantly 3 photoelectron level, afterpulses were detected on all three tubes in the following time intervals: 52 - 58.5 ns; 933 - 987 ns and 8.5 - 14 μs.

Since the afterpulse time zones were fairly well defined from tube to tube, gating could be done in signal processing almost completely eliminating the error that might otherwise be caused by the afterpulses.

Acknowledgements

This work was performed as part of the program of the Electronics Research and Development Group of the Lawrence Berkeley Laboratory, University of California, Berkeley, California, and was partially supported by the Director, Office of Energy Research, Office of High Energy Nuclear Physics, Division of High Energy Physics of the U.S. Department of Energy under Contract No. W-7405-ENG-48 and by the DUMAND Hawaii Center, University of Hawaii, Honolulu, Hawaii.

References

1. A. Roberts, G. Wilkins, The 1978 DUMAND "Standard" Array. Proceedings of the 1978 DUMAND Summer Workshop, Vol. 3, pp. 9-22.

2. H. Hinterberg, A. Roberts, F. Reines, Improvements in the 1978 Standard DUMAND Module: Sea Urchin, Proceedings of the 1979 DUMAND Workshop held in Khabarovsk, Siberia, U.S.S.R.

3. J.G. Learned, Trigger Rate Considerations for the 1978 DUMAND Summer Study Model Array, Proceedings of the 1978 DUMAND Summer Workshop, Vol. 1, pp. 147-163.

4. B. Leskovar, Photomultiplier Characteristics Considerations for the Deep Underwater Muon and Neutrino Detection System, LBL-10547. Proceedings of the 1980 Deep Underwater Muon and Neutriono Detection Signal Processing Workshop (A. Roberts, Editor), Hawaii DUMAND Center, University of Hawaii, pp. 21-40, 1980.

5. C.C. Lo, P. Lecomte, B. Leskovar, Performance Studies of Prototype Microchannel Plate Photomultipliers, IEEE Trans Nucl. Sci., NS-24, No. 1, pp. 302-311, February, 1977.

6. C.C. Lo, B. Leskovar, Evaluation of the Amperex 57TVP Photomultiplier, Lawrence Berkeley Laboratory Report LBL 5328, 1976.

7. B. Leskovar, C.C. Lo, Performance Studies of Photomultipliers Having Dynodes with GaP(Cs) Secondary Emitting Surface, IEEE Trans. Nucl. Sci., NS-19, No. 3, pp. 58-62, 1972.

8. G.A. Morton, H.M. Smith, R. Wasserman, Afterpulses in Photomultipliers, IEEE Trans. Nucl. Sci., NS-14, No. 1, pp. 443-448, 1967.

9. C.C. Lo, B. Leskovar, Evaluation of the C70133B Photomultiplier with a Cesiated Gallium-Phosphide First Dynode, Lawrence Berkeley Laboratory Engineering Note EE-1387, October, 1971.

Table 1. Anode Dark Pulse Count at Different Photoelectron Levels

	Dark Pulse Count (cps)[a]												% of dark pulses from 2 to 16 photoelectron levels	% of dark pulses from 3 to 16 photoelectron levels
	Photo-electron level	1/8	1	2	3	4	5	6	7	8	9	10		
Photomultiplier Serial No.														
13370		137	71	6.6	5	3.3	2.2	1.6	1	0.5	0.3	0.18	4.8	3.6
11894		136	62	7	5.4	4	2.5	1.3	0.6	0.23	0.1	0.05	5.1	3.9
11880		207	100	8	6.8	5.5	3.8	2.4	1.1	0.4	0.2	0.1	3.86	3.23

[a] Dark pulse summation is defined by $\sum_{N \text{ photoelectrons}}^{16 \text{ photoelectrons}} = \text{counts per second}$

where N = 1/8, 1, 2, ...10

Table 2. Signal Induced Anode Pulse Count Rate at Different Photoelectron Levels

	Induced Pulse Count (cps)[a]												% of anode pulses from 2 to 16 photoelectron levels	% of anode pulses from 3 to 16 photoelectron levels
	Photo-electron level	1/8	1	2	3	4	5	6	7	8	9	10		
Photomultiplier Serial No.														
13370		106k	58k	63k	0.74k	91	16	4	1.3	0.37	0.26	0.14	5.9	0.7
11894		107k	54k	4.7k	0.57k	63	11.5	3.2	1	0.36	0.21	0.1	4.4	0.53
11880		110k	53k	5k	0.58k	112	18	5.5	1.76	0.7	0.36	0.2	4.5	0.52

[a] Anode pulse summation is defined by $\sum_{N \text{ photoelectrons}}^{16 \text{ photoelectrons}}$ = counts per second

where N = 1/8, 1, 2, . . . 10

Table 3. Afterpulse Performance of 8854 Photomultiplier

		Photomultiplier Serial No. 11370			Photomultiplier Serial No. 11894			Photomultiplier Serial No. 11880		
Afterpulse Count Rate (cps)	Measurement Time Interval	0-680ns	450ns-7μs	4.5μs-68μs	0-680ns	450ns-7μs	4.5μs-68μs	0-680ns	450ns-7μs	4.5μs-68μs
	Single Photoelectron Pulse Rate=100kHz	120 at 54.5ns 30 at 192ns	b	b	106 at 58.5ns 5.5 at 190ns	b	b	145 at 52ns 8 at 190ns	b	b
	Single Photoelectron Pulse Rate=10kHz	b	a	b	b	0.8 at 933ns	b	b	a	b
	Single Photoelectron Pulse Rate=1kHz	b		3.4 at 12.5μs	b		a	b		a
	Three Photoelectron Pulse Rate=10kHz	12.5 at 55ns 6.4 at 197ns	1.8 at 966ns	72 at 12.8μs[c]	10.4 at 59ns 12 at 198ns	2 at 956ns	9 at 9.2μs 14 at 14μs	4 at 54.5ns	4 at 987ns	68 at 8.5μs 54 at 12.8μs

a - Afterpulses were not observed.
b - Measurement was not made due to a measuring system limitation.
c - Avarage distribution width was 5.3μs, FWHM.

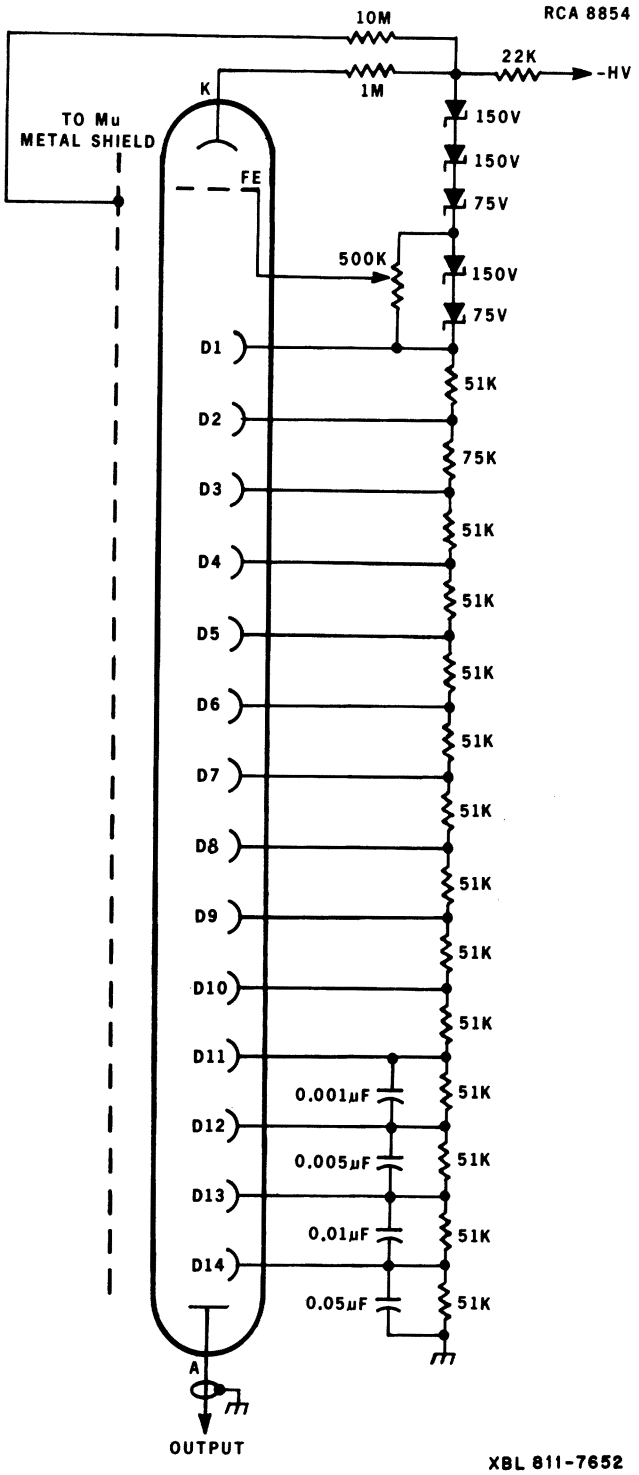

Fig. 1 Schematic diagram of voltage divider.

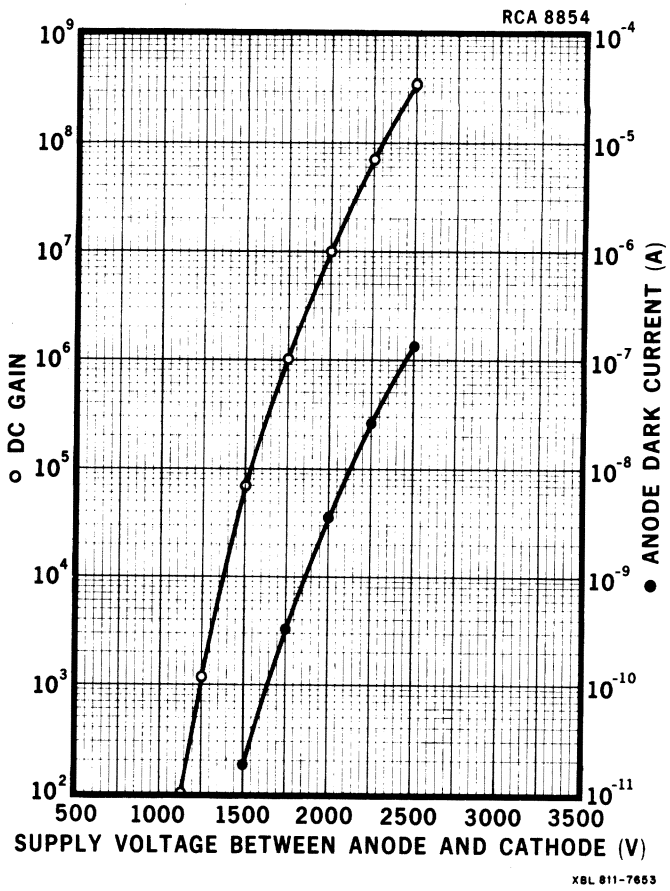

Fig. 2 Gain and dark current of 8854 as a function of supply voltage between anode and cathode.

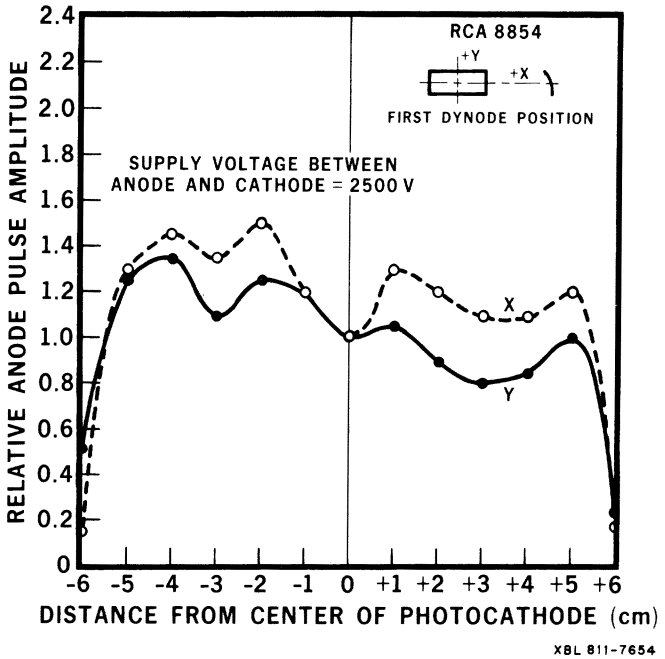

Fig. 3 Collection and quantum efficiency uniformity as a function of the position of the photocathode sensing area for RCA 8854, S/N 11894.

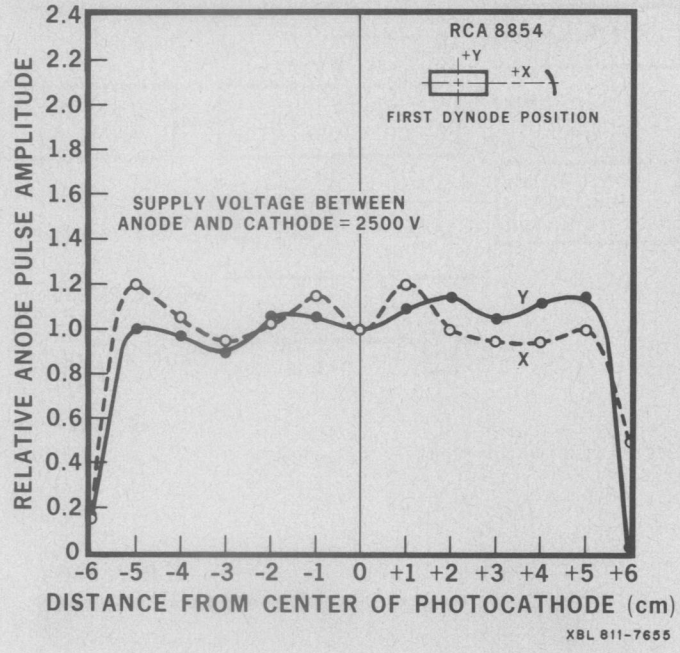

Fig. 4 Collection and quantum efficiency uniformity as a function of the position of the photocathode sensing area for RCA 8854, S/N 13370.

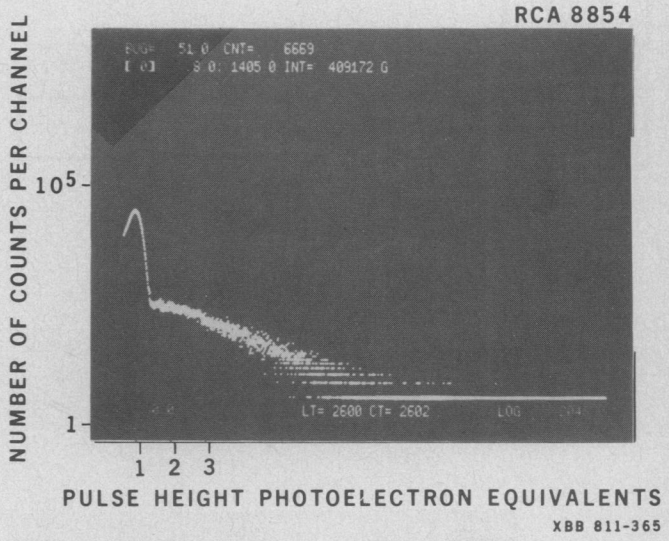

Fig. 6 Typical dark pulse spectrum of 8854.

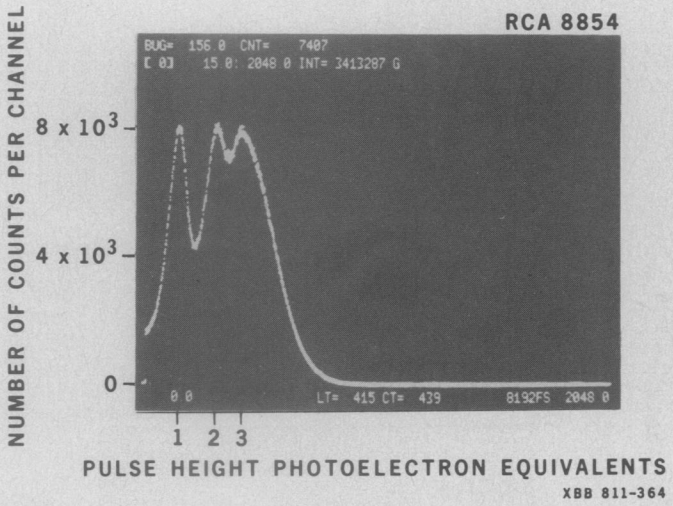

Fig. 5 Typical pulse height resolution of 8854.

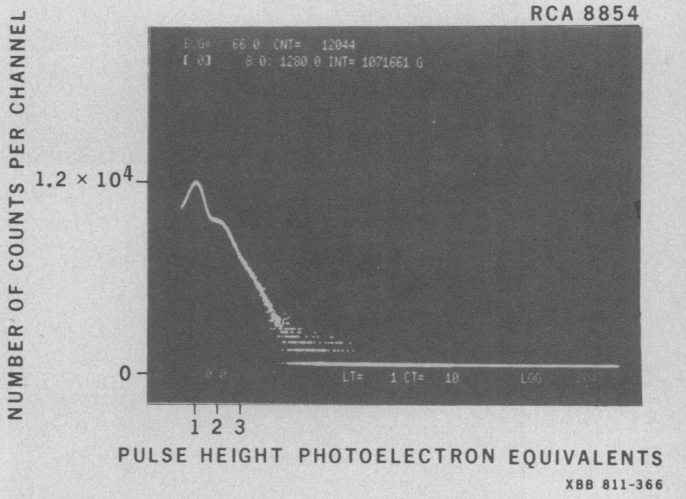

Fig. 9 Pulse height spectrum with 100 KHz signal-induced count rate.

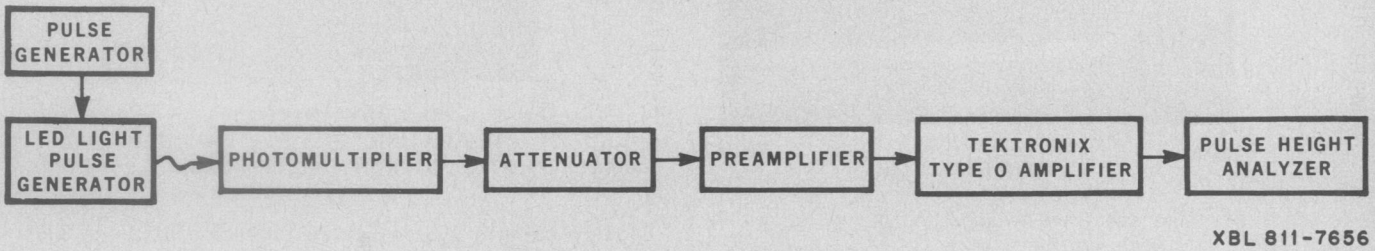

Fig. 7 System block diagram for measuring pulse height spectrum.

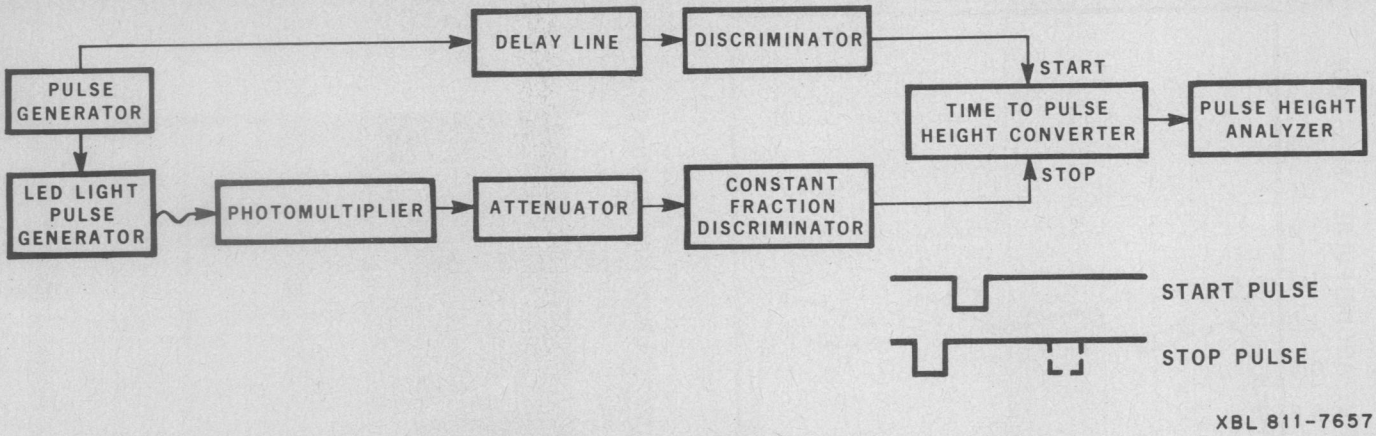

Fig. 8 System block diagram for measuring time spectrum of afterpulse.

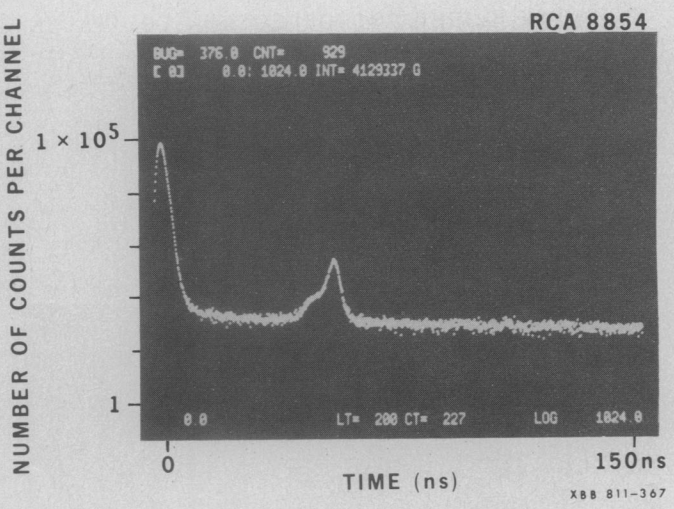

Fig. 10 Time spectrum of anode output pulse between 0-150ns.

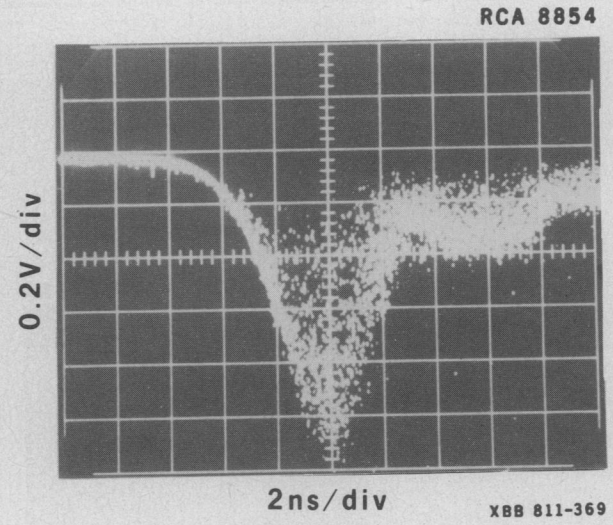

Fig. 12 Single photoelectron pulse response of 8854.

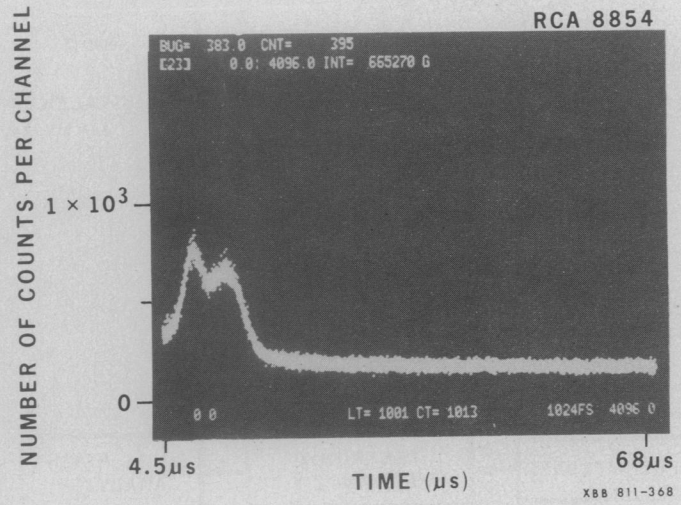

Fig. 11 Time spectrum of anode output pulse between 4.5-68μs.

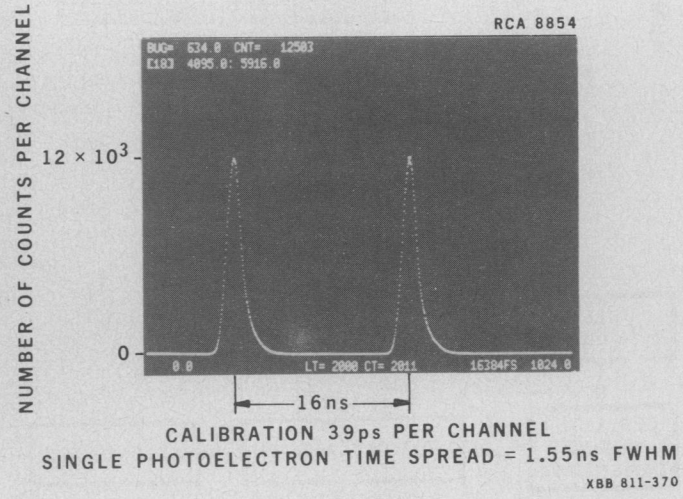

Fig. 13 Single photoelectron time resolution of 8854.